Average Power Handling Capability of Microstrip Passive Circuits Considering Metal Housing and Environment Conditions

Miguel Á. Sánchez-Soriano, *Member, IEEE*, Yves Queré, *Member, IEEE*, Vincent Le Saux, Cédric Quendo, *Member, IEEE*, and Stephane Cadiou

***Abstract*— In this paper, the average power handling capability (APHC) of microstrip passive circuits considering the metal housing and environment conditions is investigated in detail. A systematic method is proposed for the computation of the APHC of microstrip circuits in open and enclosed metal housing configurations, typically used in microwave components. The method also yields an estimate of the maximum temperature in a microstrip circuit for a given input power. Closed-form equations accounting for external conditions, such as convection or radiation heat transfer are given to evaluate the APHC. For validation, two microstrip bandstop filters centered at 10 GHz are analyzed following the proposed model, and the results are compared with those simulated showing a good agreement. In addition, both circuits are fabricated and characterized. Thermal profile measurements are provided, confirming the predicted results. The effect of the topology layout and the electromagnetic performance on the APHC are also discussed.**

***Index Terms*— Average power handling capability (APHC), electrothermal analysis, metal housing, microwave devices, planar circuits, power applications.**

I. Introduction

MICROSTRIP passive circuits are an essential part in transmitter and receiver systems. They generally manage signal transmission between stages, filtering, and/or power division. Microstrip circuits may limit the maximum working power of the communication system. Their maximum power handling capability can be determined by the heating in the materials (related to the ohmic and dielectric losses), which limits average power handling capability (APHC), and by the dielectric breakdown field (related to the maximum peak voltage that the dielectric can withstand) limiting the peak power handling capability. Other effects such as nonlinear effects in the materials and/or the multipaction effect (more characteristic of waveguide technology in spatial high-power applications) can also limit the maximum working power [1], [2]. Losses in microstrip circuits can be important, and especially as the working frequency increases. In addition, there is currently an increasing tendency toward the miniaturization that directly affects the thermal performance of the circuits. All these factors make the study of APHC in microstrip devices of great interest.

The APHC of microstrip lines was first studied in [1] and [3]. Later on, different works dealt with APHC for microstrip coupled lines [4], [5], coupled-line filters [6], [7], multilayer microstrip lines [8], and thin-film microstrip lines [9]–[11]. Basically, the procedure for its calculation is to determine the conductor and dielectric losses, then, the heat flow distribution in the microstrip cross section is derived to finally obtain the temperature rise that defines the maximum working input power. In all these works, a reference temperature on the ground (typically fixed as the ambient temperature) is assumed, and the generated heat flow is considered concentrated in the strip-to-ground region. In this paper, and unlike in other papers, the effects of the metal housing and environment conditions in the microstrip circuit are studied and considered for the calculation of the APHC. It is shown that the external conditions can strongly affect the obtained APHC value, and therefore, are very important to be considered in a realistic situation. A systematic method is proposed for the analytical calculation of the APHC considering external conditions. This method is validated through the electrothermal simulations (by means of a multiphysics simulator) of different microstrip passive circuits. In addition, as a differentiating element with respect to previous works, thermal profile measurements have been carried out corroborating the predicted results with the proposed model.

This paper is organized as follows. In Section II, the two conventional microstrip configurations (with open and enclosed metal housing) are presented and analyzed. The theoretical electrothermal analysis is described, including the analysis of the external conditions for each geometry and their distinct features. In Section III, the procedure to calculate the APHC (or the maximum temperature for a given input signal power) of a whole microstrip passive circuit is detailed.

Manuscript received January 17, 2014; revised July 16, 2014; accepted July 22, 2014. Date of publication August 25, 2014; date of current version October 3, 2014. This work was supported by the Euripides European Project MIDIMU-HD. Recommended for publication by Associate Editor A. Shapiro upon evaluation of reviewers' comments.

M. Á. Sánchez-Soriano, Y. Queré, and C. Quendo are with the Laboratoire des Sciences et Techniques de l'information, de la Communication et de la Connaissance, Université de Bretagne Occidentale, Brest 29238, France (e-mail: m.sanchez.soriano@ieee.org; yves.quere@univbrest.fr; cedric.quendo@univ-brest.fr).

V. Le Saux is with the Laboratoire Brestois de Mécanique et des Systémes, ENSTA Bretagne, Brest 29806, France (e-mail: vincent.le_saux@ensta-bretagne.fr).

S. Cadiou is with Thales Communications and Security, Cholet 49300, France (e-mail: stephane.cadiou@thalesgroup.com).

Color versions of one or more of the figures in this paper are available online at http://ieeexplore.ieee.org.

Digital Object Identifier 10.1109/TCPMT.2014.2345100

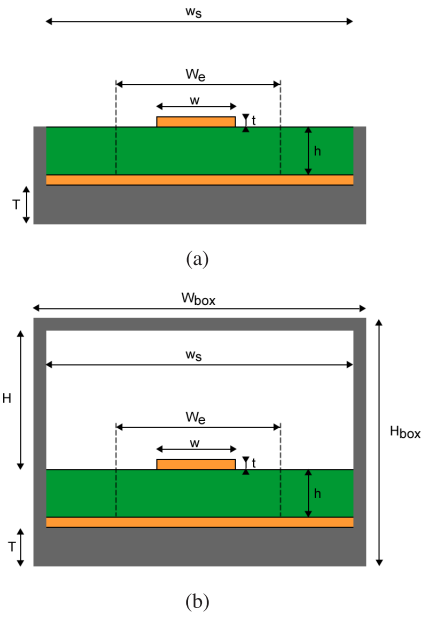

Fig. 1. Cross section of a microstrip circuit. (a) Open metal housing configuration. (b) Enclosed metal housing configuration.

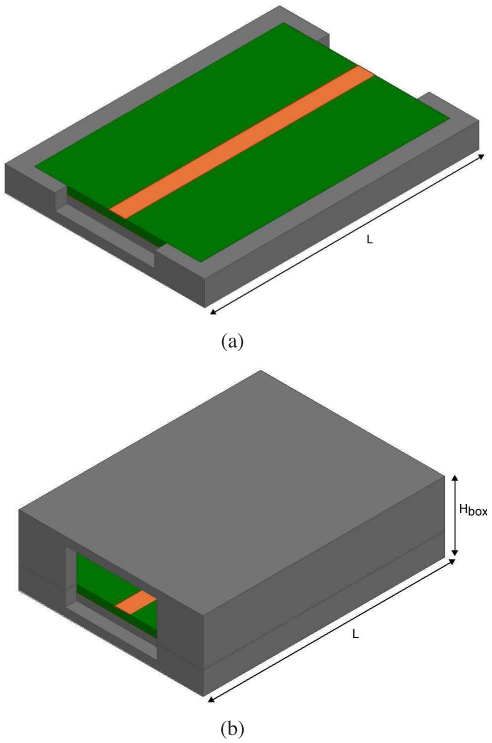

Fig. 2. 3-D scheme of a microstrip transmission line. (a) In an open metal housing configuration. (b) In an enclosed metal housing configuration. In both schemes the connector location can be noticed.

Based on this method, different circuits are analyzed and discussed. Simulation and measurement results are also provided validating the proposed method. Finally, conclusions are drawn in Section IV.

II. Description, Theoretical Analysis, and Modeling

Fig. 1 shows the cross section of a microstrip circuit with two kinds of metal housing configurations: 1) open and 2) enclosed. The structure is geometrically defined by the width w and thickness t of the strip, the width w_s and thickness h of the substrate, the dimensions W_{box} and H_{box} of the metal housing and the length of the circuit L (Fig. 2). The microstrip circuit presents metal and dielectric losses (linearly proportional to the input signal power P_{in}), which generate heat in the circuit. The generated heat produces a gradient of temperature per unit of power ΔT (°C/W) between the strip and the ground plane limiting the maximum continuous wave operation signal power (or APHC). The ΔT can be calculated as

$$\Delta T = \Delta T_c + \Delta T_d = \frac{2h}{K}\left(\frac{\mu\,\alpha_c(f)}{W_e(f)} + \frac{\eta\,\alpha_d(f)}{2W_e(f)}\right) \tag{1}$$

where ΔT_c and ΔT_d are the temperature gradients generated in the microstrip line due to conductor and dielectric losses, respectively, K is the substrate thermal conductivity, α_c and α_d are the frequency-dependent conductor and dielectric attenuation constants (in Np/m) for a uniform line, and W_e is the thermal effective microstrip width based on a parallel-plate waveguide model. This equation is derived from [3] with the inclusion in this paper of two additional adimensional parameters μ and η to account for the variation of the power loss with the position in microstrip circuits different from matched lines, where $\mu = \eta = 1$. As an example, in a short-circuited (or open-circuited) transmission line, a standing wave is formed along the line where maximum values of voltage and current are clearly defined. At the points of maximum current we have $\mu = 2$ and $\eta = 0$, whereas at the points of maximum voltage, $\mu = 0$ and $\eta = 2$; in a coupled-line filter μ and η depend on the position along the resonators, the fractional bandwidth, and the interresonator coupling distribution [6], and so on. It is worth mentioning that in this calculation two assumptions are made: 1) $(\alpha_c + \alpha_d)L \ll 1$, so that α_c and α_d are independent of the propagation direction and only the electromagnetic behavior of the device (by means of μ and η) defines the dependence of ΔT with the propagation direction and 2) all generated heat flow is assumed to be concentrated in the region defined by W_e and the heat flux going out through the surface layers by convection and/or radiation is considered negligible. The validity of the latter assumption is discussed later on both for the open and enclosed housing configurations.

Once ΔT is known, the APHC is obtained as

$$P_{\max}(f) = (T_{\max} - T_{\text{ref}})/\Delta T(f) \tag{2}$$

where $T_{\max}$ is the maximum temperature of operation, which can be defined as that temperature where the circuit changes its electrical and mechanical performances (in general, the substrate glass transition temperature) or that temperature which produces an excessive thermal stress in the circuit. In all previous works T_{ref} is set as a given constant temperature (generally, the ambient temperature T_{amb}). However, for medium-to-high power applications T_{ref} can be further different from T_{amb}, leading to a much lower APHC.

For this reason, it is essential to find a systematic method to estimate this temperature whose value is influenced by the metal housing and environment conditions (convection and radiation boundary conditions) as well as by P_{in}.

For the calculation of T_{ref}, the heat propagation in the metal housing needs to be evaluated. If the metal housing is thick enough, it can act as a good thermal spreader equalizing the temperature on the ground plane and also in the substrate volume outside the region delimited by W_e, as observed in Fig. 1. This statement comes from the fact that the gradient of temperature created in the metal housing mainly depends on three factors: 1) boundary conditions on the outside surface layers; 2) thermal material resistance; and 3) thermal spreading/constriction resistance. As studied in [12]–[14], for a fixed heat source area (in our case, the microstrip circuit area) and for low Biot numbers (meaning conduction is the main mechanism of heat transfer in the structure), the spreading resistance decreases as the metal housing thickness T increases, down to reach a constant value independent from both the metal housing thickness and the boundary conditions. In the case under study, i.e., for high frequency applications, the housing geometrical dimensions (T, W_{box}, and L) are in the order of millimeter (or a few centimeter), so that the spreading resistance reaches its minimum value, and the thermal conductivity of the metal housing is typically higher than 100 W/m·°C (200 W/m·°C for aluminum metal housing, which is broadly used due to its low cost and weight and its high resistance to corrosion). These values lead to the thermal material and spreading resistances to be negligible in comparison with the thermal resistance associated to the boundary conditions. Therefore, it can be assumed that the temperature is practically homogeneous both in the metal housing and the ground plane, and its value mainly depends on the boundary conditions and the heat generated by the microstrip circuit. In addition, as the Biot numbers in all surface layers are low, the heat flow lost by convection (and also by radiation) can be considered to be isoflux. Hence, outside the surface delimited by W_e, using the Newton law of cooling in combination with an energy balance, it can be written that

$$Q_{\text{int}} + Q_{\text{ext}} = \sum_{i=1}^{n} h_{\text{conv},i}\, A_i\, (T_{\text{ref}} - T_{\text{amb}}) + \sum_{j=1}^{m} h_{\text{rad},j}\, A_j\, (T_{\text{ref}} - T_{\text{amb}}) \tag{3}$$

where Q_{int} is the whole internal loss of the circuit (not accounting for radiation loss[1] since they do not generate any heat in the circuit), Q_{ext} is any external heat source (such as solar radiation), n and m are the number of surfaces layers (A_i and A_j) exposed to convection and radiation boundary conditions, respectively, and h_{conv} and h_{rad} are the convection and radiation coefficients. The values h_{conv} and h_{rad} depend on the external conditions of each layer, i.e., if there is a heat sink attached, natural or forced convection, emissivity and so on, as will be seen later on.

By combining (2) and (3), and defining Q_{int} as $Q_{\text{int}} = \Gamma P_{\text{in}}$, the APHC can be calculated as

$$P_{\max} = \frac{T_{\max} - T_{\text{amb}} - Q_{\text{ext}}/\Lambda}{\Delta T + \Gamma/\Lambda} \tag{4}$$

where

$$\Lambda = \sum_{i=1}^{n} h_{\text{conv},i}\, A_i + \sum_{j=1}^{m} h_{\text{rad},j}\, A_j \tag{5}$$

and

$$\begin{aligned}\Gamma &= \Gamma_{\text{total}} - P_{\text{rad}} \\ &= 1 - 1/\text{IL (linear)} - 1/\text{RL (linear)} - P_{\text{rad}}\end{aligned} \tag{6}$$

where Γ_{total} refers to the total loss factor in the device (accounting for all loss mechanisms), insertion loss (IL) and return loss (RL) denote insertion loss and return loss of the whole circuit, respectively, and P_{rad} denotes the radiation loss factor.

A. Open Metal Housing Configuration

For the case of a microstrip circuit in an open metal housing configuration, as shown in Figs. 1(a) and 2(a), the microstrip circuit surface layer is directly exposed to natural (or forced) convection and is able to radiate/absorb energy by thermal radiation to/from the environment. The metal housing bottom layer could be attached to a heat sink providing an equivalent convection coefficient, whereas the remaining layers of the metal housing are also exposed to convection and radiation heat transfer mechanisms. The convection coefficient of each layer is a function of the Grassoft number (for free convection), and/or of the wind velocity through the Reynolds number (for forced convection), and also depends on the inclination of the configuration (horizontal, vertical, or inclined). Their values can be extracted from the empirical results given in [15].

Regarding thermal radiation, all exposed outside layers radiate according to the infrared emissivity ϵ (on what follows, just emissivity) of the metal housing, the strip conductor, and the dielectric at the temperature T_{ref},[2] presenting an associated radiation heat transfer coefficient (linearized via a first-order Taylor series expansion)

$$h_{\text{rad},i} = \sigma \epsilon \frac{\left(T_{\text{ref}}^4 - T_{\text{amb}}^4\right)}{\left(T_{\text{ref}} - T_{\text{amb}}\right)} \approx 4\sigma \epsilon_i T_{\text{amb}}^3 \tag{7}$$

where σ is the Stefan–Boltzmann constant and ϵ_i is the emissivity of the considering surface i. In addition, some layers could receive solar radiation G_s, weighted by the solar absorptivity α_s of each layer.

[1]The term radiation loss refers to the power loss by electromagnetic radiation from the microstrip device at the working operation frequency due to the fact that its electromagnetic fields are not enclosed. This term must not be confused with the thermal/infrared radiation (or just radiation), used throughout this paper.

[2]It is assumed $T_{\text{ref}} > T_{\text{amb}}$, which leads the outside layers to radiate. The opposite temperature relation means that the outside layers receive energy by radiation from the environment (infrared), without any loss of generality in (3).

Special attention must be paid to the microstrip surface, since there are two materials (with different properties and temperatures) involved in the heat propagation with the environment. In the microstrip circuit surface, the energy (per unit length) delivered to the environment can be written as (assuming constant heat flux both in the metal and the dielectric)

$$q = h_{\text{conv}} W_e (T_{w_e} - T_{\text{amb}}) + h_{\text{conv}} (w_s - W_e)(T_{\text{ref}} - T_{\text{amb}}) + h_{\text{rad},w_e} W_e (T_{w_e} - T_{\text{amb}}) + h_{\text{rad},w_s} (w_s - W_e)(T_{\text{ref}} - T_{\text{amb}}) \tag{8}$$

where T_{we} is the temperature in the surface delimited by W_e, and h_{rad,w_e} and h_{rad,w_s} are the radiation coefficients associated to the strip and dielectric in an open environment. In general, $W_E \ll w_s$, thus, (8) can be simplified to

$$q \approx (h_{\text{conv}} + h_{\text{rad},w_s}) w_s (T_{\text{ref}} - T_{\text{amb}}). \tag{9}$$

B. Enclosed Metal Housing Configuration

In the case of an enclosed metal housing configuration between the microstrip circuit surface layer and the metal housing top cover there can be some air producing cooling by convection. However, for typical microstrip metal housing, where H should be around five times h (to avoid any parasitic coupling between the microstrip mode and the enclosure), the Rayleigh number is small (generally lower than the critical number 1708), meaning that the viscous forces are dominant versus the inertial forces, and therefore, leading to a regime of heat transfer by pure conduction through the air. Thus, since the air thermal conductivity is very low ($k_{\text{air}} \sim 0.026$ W/m·°C), the cooling by convection/conduction through this layer can be ignored and not considered in (3). The convection heat transfer of the outside metal housing surfaces is treated as in the previous case.

With respect to the radiation performance, the outside surface layers radiate to the surroundings according to the emissivity of the metal housing at T_{ref}, and again, they could receive solar radiation. Inside the enclosure, there are six faces involved in the radiation mechanism, however, the radiation interchange between perpendicular layers is not generally significant due to their low view factors, and only the radiation between the microstrip circuit layer and the inside top cover is considered. It should be noted that in the proposed configuration, the net radiated energy by the microstrip circuit is absorbed by the inside top cover, hence, the energy balance is null and it does not affect the calculation of T_{ref} using (3). Anyway, it is important to calculate this net energy radiated by the microstrip circuit layer to know the limit of (1) to be used as a good approximation of the temperature rise ΔT. The microstrip radiated energy (per unit length) can be derived from the conventional two-surface radiation heat transfer problem [15] as

$$q_{\text{rad}} \approx \frac{\sigma \left(T_{w_e}^4 - T_{\text{ref}}^4\right)}{\dfrac{1-\epsilon_{w_e}}{W_e\,\epsilon_{w_e}} + \dfrac{1-\epsilon_{\text{in}}}{w_s\,\epsilon_{\text{in}}} + \dfrac{1}{W_e\,F_{12}}} = h_{\text{rad},w_e}^{\text{encl}}\, W_e (T_{w_e} - T_{\text{ref}}) \tag{10}$$

where ϵ_{w_e} and ϵ_{in} are the emissivities associated to W_e and the inner top cover (which can be that of a electromagnetic absorber), respectively, and F_{12} is the view factor from the microstrip circuit surface to the inner top cover (whose value is near 1 for microstrip configurations with H/L, $H/w_s \ll 1$). As deduced from (10), it is assumed that only the area delimited by W_e radiates because the remaining substrate area stays at T_{ref} (the same as the metal housing). This is not the case for the open metal housing configuration, where the whole microstrip circuit surface presents a temperature greater than T_{amb} and thus, is able to radiate to the surroundings.

The validity of (1) is, therefore, subject to the fulfillment of the following condition $\Delta T \ll 1/(h_{\text{rad},w_e}^{\text{encl}}\, W_e)$, as it means that the generated heat flux mainly propagates along the microstrip circuit thickness. In any other case, (1) will overestimate the temperature gradient produced in the circuit since radiation will be playing an important role in the circuit's cooling. For the open housing configuration, convection on the microstrip layer must be added to the aforementioned condition as

$$\Delta T \ll \frac{T_{w_e} - T_{\text{ref}}}{T_{w_e} - T_{\text{amb}}} \cdot \frac{1}{(h_{\text{rad},w_e} + h_{\text{conv}})\, W_e}. \tag{11}$$

III. Results and Discussion

The suggested procedure to calculate the APHC of a microstrip passive circuit and to predict its maximum temperature for a given input power considering the effects of the metal housing and environment, can be summarized as follows.

1) Identify all parts of the passive microstrip circuit under study (transmission lines, stubs, couplers, resonators, etc.).
2) Compute the maximum gradient of temperature ΔT for each part of the circuit by means of (1) at the frequency of interest, considering the parameters μ and η, which depend on the electromagnetic behavior of each part.
3) Find the IL and RL of the whole circuit at the frequencies under study, to compute Γ. In this step, a full wave simulator may be needed, especially for complex structures.
4) Following the guidelines given in Section II, and considering the kind of housing and the environment conditions, proceed as follows (depending on the goal). If the objective is to obtain the APHC, it is directly computed using (4) after previously setting T_{max}. On the other hand, if T_{max} is to be known for a given P_{in}, T_{ref} can be directly calculated from (3), and after that, T_{max} of the circuit is obtained from (2), where $P_{\text{max}} = P_{\text{in}}$ is set.

To validate the proposed method, some microstrip circuits have been analyzed and the predicted results have been compared with those simulated and measured. The circuits have been designed and implemented on Megtron 6 substrate, from Panasonic, which has the following characteristics: $\epsilon_r = 3.6$, $K = 0.4$ W/m·°C, $\tan\delta = 0.006$, $h = 0.93$ mm, and $t = 38$ μm, with copper as metal layer. The emissivities for the dielectric and copper are set as 0.85 and 0.2, whereas the solar absorptivity of aluminum is fixed as 0.2.

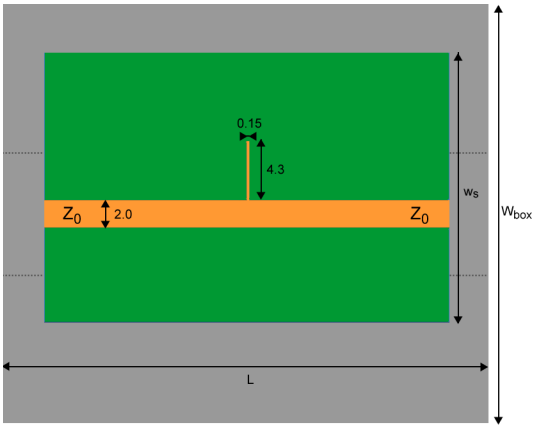

Fig. 3. Layout of the first-order narrowband bandstop filter. $W_{box} = 30$ mm, $w_s = 20$ mm, $L = 36$ mm, and $T = 5$ mm. In addition, for the enclosed metal housing configuration: $H = 5$ mm and $H_{box} = 12$ mm. Units shown in the picture are in millimeters.

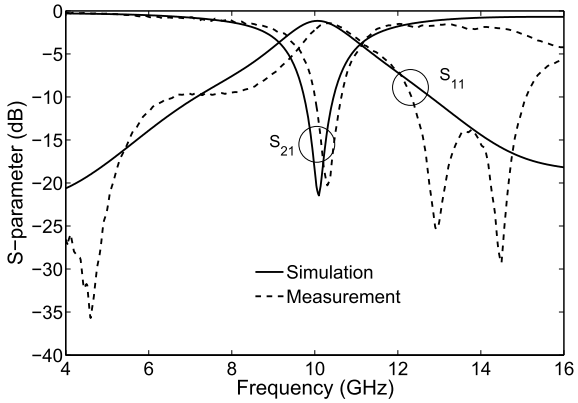

Fig. 4. Simulated and measured responses of the first-order narrowband bandstop filter. Measured 10 dB relative stopband bandwidth $BW_{10dB} = 6\%$.

A. Example 1: First-Order Narrowband Bandstop Filter

A first-order narrowband bandstop filter is first considered for its analysis. The top view of the circuit can be observed in Fig. 3. The filter is designed to present a transmission zero at 10.0 GHz, at the frequency where the open-circuited stub measures a quarter-wavelength. Fig. 4 shows the full wave simulated (using HFSS) and measured responses of the filter. At the design frequency (10 GHz), a standing wave is formed in the open-circuited stub as well as in the feeding lines. The maximum ΔT occurs in the open stub due to its higher attenuation constant and lower effective width ($W_e = 1.58$ mm at 10 GHz for the open stub). In particular, it occurs near the stub's open-circuited termination, where there is a maximum of electric field, since at this frequency, dielectric losses are more important than conductor losses (at 10.0 GHz, $\alpha_c = 0.59$ Np/m, and $\alpha_d = 0.79$ Np/m for the stub). For the ΔT computation, the average attenuation constants in the open-circuited stub-based resonator are used in (1), which are calculated in a similar fashion as in [6], as $\overline{\alpha_{c,d}} = (2Z_{stub}/Z_0)\alpha_{c,d}$, where Z_{stub} and Z_0 are the characteristic impedances of the stub and feeding lines, respectively. Near the open-circuited termination, $\mu = 0$ and $\eta = 2$, and ΔT is accordingly calculated at 10.0 GHz as $\Delta T = 7.8$ °C/W. The whole losses in the circuit at 10.0 GHz including losses in the feeding lines are found to be $Q_{int} = \Gamma P_{in} = 0.123 P_{in}$. Next, two situations are considered, open and enclosed metal housing configurations. For both situations, $T_{amb} = 22$ °C and natural convection heat transfer is assumed with $h_{conv} = 9$ W/m^2·°C for all surfaces (as seen later, this value corresponds to the estimated convection coefficient value in the laboratory environment). Radiation is only considered in the dielectric due to the low emissivity of copper and aluminum. In this first test, no solar absorption is considered, thus, $Q_{ext} = 0$. For the dimensions given in the caption of Fig. 3, and for an input power of 2 W, T_{ref} is found to be 31.2 °C for the open metal housing configuration and $T_{ref} = 29.3$ °C for the enclosed one. Hence, according to Section II the maximum temperatures in the circuit for each case are 46.8 °C and 44.9 °C, respectively. These predicted results agree very well with those obtained with Ansys Multiphysics (platform combining HFSS and Ansys mechanical), with a difference of <5%. It should be noted that for both situations, the area subject to convection is similar, 2952 mm^2 for the open and 3744 mm^2 for the enclosed configuration. For this reason the calculated temperatures are also close, although they are slightly lower for the enclosed configuration due to its bigger outside area. This slight temperature difference between configurations will increase as the input signal power rises.

1) Measurement Setup: To confirm the proposed model, a measurement setup has been arranged to measure the thermal profile of the circuit with an infrared camera model SC7600BB from FLIR systems for the two metal housing configurations (Fig. 5). In comparison to using thermal probes (thermocouples) for measuring the temperature, the infrared measurement by means of the thermal camera is a nonintrusive measured method. Therefore, the circuit electromagnetic field distribution (which defines the thermal profile) is not perturbed at all, which is fundamental to be accurate in this kind of measurements where only passive components are involved. Furthermore, using the infrared camera, the thermal profile in the whole circuit area can be measured providing a very valuable information. In this measurement setup, a continuous signal has been applied to the circuit at the frequency of interest. For all circuits under analysis the thermal steady-state behavior is reached after 900 s the signal generator is switched ON. For the case of the enclosed configuration, once the steady state is reached, the top cover is removed and the circuit thermal profile is immediately recorded. The circuit in this measurement setup is suspended 5 cm above the table, and thus, all its layers are subject to natural convection (as previously assumed). The convection coefficient has been experimentally estimated by means of the measured and simulated cooling time curves of the circuit alone, i.e., without the metal housing. Fig. 6 shows, during the first 7 s after the signal is OFF, the measured cooling time curve agrees reasonably well with that simulated with $h_{conv} = 9$ W/m^2·°C. Beyond this time, the measured curve follows a different tendency than those simulated, mainly due to the influence of the SMA connectors, which are not included in the simulations

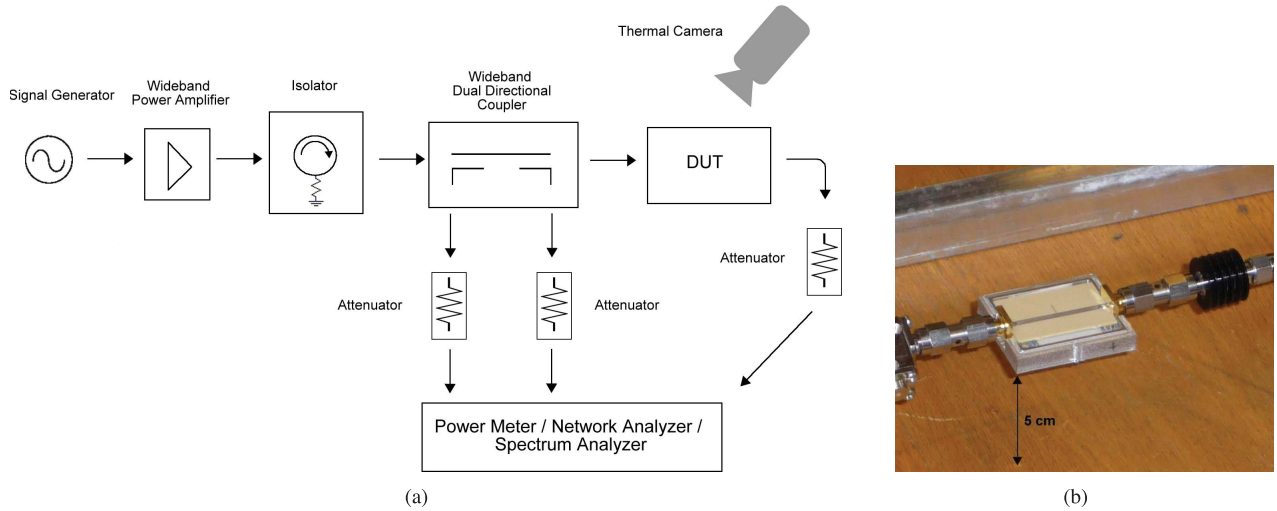

Fig. 5. (a) Measurement setup for the characterization of the device under test. (b) Photograph of one of the measured devices.

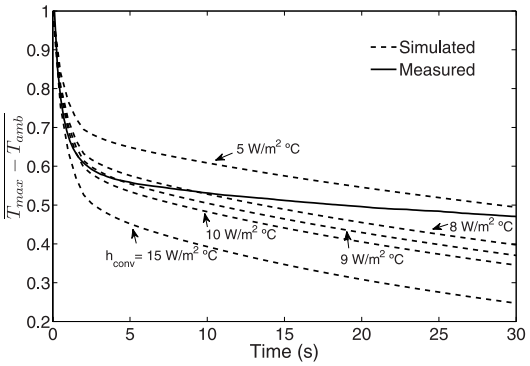

Fig. 6. Simulated and measured cooling time curves, under varied h_{conv}.

and decelerate the cooling process. Consequently, it can be concluded that h_{conv} is roughly 9 W/m^2·°C in the laboratory environment [16].

A compensated nonuniformity correction has been applied to correct the camera sensors heterogeneities. As an infrared camera measures thermal radiation and not directly temperature, the most common approach in infrared measurements to get accurate results consists in spraying black paint over the surface of the samples of interest to minimize the influence of the environment by maximizing the emissivity of the sample. Here, no specific preparation of the sample is applied (because the paint could affect the electromagnetic behavior of the circuit) and a correction has been done before the interpretation of the measurement as follows. Assuming the circuit as opaque, the thermal radiation measured by the infrared camera, while looking at the circuit can be written as

$$\Phi_{\text{total}} = \varepsilon \Phi_{\text{circuit}}(T_{\text{circuit}}) + \rho \Phi_{\text{amb}}(T_{\text{amb}}) \tag{12}$$

where ε is the emissivity of the circuit (and depends on the location) and ρ is the reflection coefficient. The real flux emitted by the circuit can be extracted

$$\Phi_{\text{circuit}}(T_{\text{circuit}}) = \frac{1}{\varepsilon}[\Phi_{\text{total}} - (1-\varepsilon)\Phi_{\text{amb}}(T_{\text{amb}})]. \tag{13}$$

A classical sixth-order polynomial is finally used to convert the measured flux into temperature. It should be noted that to simplify the problem, a constant emissivity of 0.85 has been considered in all the circuit, which means that the temperature value within the metal part of the circuit is underestimated and therefore not evaluated properly (a discontinuity of the thermal signal at the interface of the substrate and the conductor will be noticed in the measured thermal profiles). This is not a big issue since the temperature around the line delimited by W_e (which involves both substrate and metal) is practically constant. Therefore, the temperature can be actually evaluated in the substrate region close to the metal without affecting the accuracy of the measurement results.

Fig. 7 shows the simulated and measured thermal profiles obtained for the open configuration at 10.0 GHz. The thermal profile has also been measured at 10.2 GHz (where the transmission zero appears in the measured response) resulting in practically the same profile. The maximum hot spot can be clearly identified close to the stub open-circuited termination, as predicted. Only small differences are found between both profiles, completely validating the proposed model. Note that as previously mentioned, the simulated results agree well with those obtained with the model. These differences are probably related to different uncertainties involved in the measurement setup: the used convection coefficient value against the real value in the laboratory environment (which can vary with the temperature), the real input power coming into the circuit or the effect of the conductive epoxy for fixing the circuit in the metal box that is not considered in the model.

Next, different scenarios are contemplated and discussed.

2) APHC at Other Frequencies: The same procedure has been repeated at 8 GHz, within the passband of the filter, where the input signal is well transmitted along the feeding lines and there is no part of the circuit resonating. Hence, at 8 GHz $\mu = \eta = 1$ along the feeding lines. The attenuation constants for the feeding lines are $\alpha_c = 0.12$ Np/m and $\alpha_d = 0.78$ Np/m. The predicted T_{max} under $P_{\text{in}} = 2$ W is 31.3 °C and 29.7 °C for the open and enclosed configurations. The measured results with the thermal camera are again very close

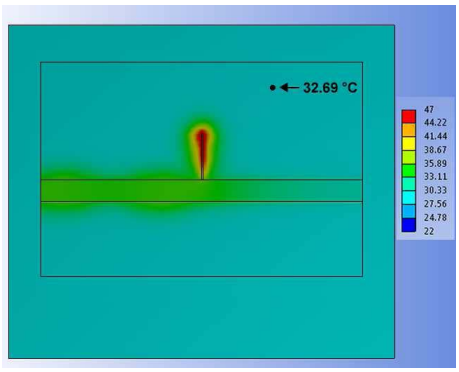

(a)

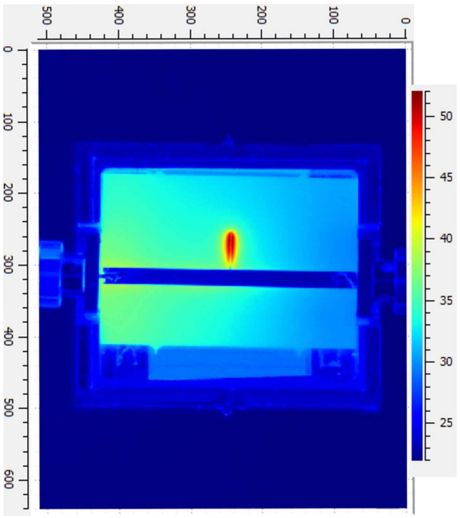

(b)

Fig. 7. (a) Simulated and (b) measured thermal profiles of the first-order narrow band bandstop filter at 10.0 GHz for the open metal housing configuration.

to those predicted: $T_{\max} = 32.1$ °C and 30.5 °C, respectively. In view of the results, this filter configuration could withstand much higher power signal levels in the passband than in the stopband. Indeed, if $T_{\max} = 80$ °C is defined as the maximum working temperature, the APHC at 8 GHz, according to (4), is 12.75 and 15.03 W (for the open and enclosed housing situations, respectively), whereas at 10.0 GHz, 4.66 and 5.06 W.

3) APHC After Attaching a Heat Sink: To increase the APHC a heat sink can be attached at the bottom of the metal housing of the filter. A commercial heat sink with an area of 35.56 mm × 35.56 mm and a thermal resistance $R_{\text{th,hs}}$ of 6.0 °C/W is used in this analysis. The equivalent convection coefficient for the bottom surface can be calculated as

$$h_{\text{eq}} = \frac{1}{A_{\text{hs}} R_{\text{th,hs}}} \tag{14}$$

resulting in $h_{\text{eq}} = 132$ W/m^2·°C. By solving (4) again, APHC at 10 GHz is found to be 6.84 and 6.86 W for the open and enclosed metal housing configurations. Therefore, attaching a heat sink makes both configurations converge to the same results, since an important part of the generated heat flux in the circuit is delivered to the heat sink, and the cooling through the remaining layers is much less significant.

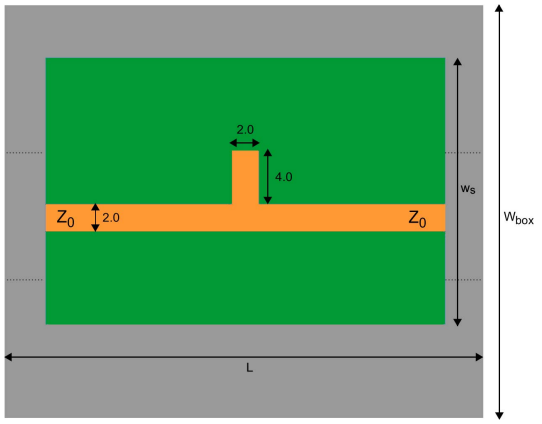

Fig. 8. Layout of the first-order wideband bandstop filter. $W_{\text{box}} = 30$ mm, $w_s = 20$ mm, $L = 36$ mm, and $T = 5$ mm. In addition, for the enclosed metal housing configuration: $H = 5$ mm and $H_{\text{box}} = 12$ mm. Units shown in the picture are in millimeters.

4) APHC Using the Conventional Approach: As an illustration, the APHC is also calculated at the resonant frequency of the aforementioned circuit using the conventional approach, i.e., without including any external and boundary conditions in the model and with $T_{\text{ref}} = T_{\text{amb}} = 22$ °C. In such a case, APHC is 7.44 W, which means a value 60% and 47% higher than those calculated and validated in the proposed model for the open and enclosed configurations, respectively. This confirms that accounting for the external conditions is essential to keep the microstrip circuits in safety ranges of input power.

5) Circuit Placed Outside: In the case when the circuit is placed outside (only the enclosed metal housing configuration is considered in that situation), it could be exposed to solar radiation. For a solar radiation of $G_s = 800$ W/m^2, and assuming that only the metal top layer receives this radiation with an angle of 20° respect to the sun (the remaining parameters regarding convection and infrared radiation remain the same as in the previous case), $Q_{\text{ext}} = \alpha_s G_s \cos 20°(W_{\text{box}} L) = 0.16$ W, leading to a predicted APHC of 13.77 W at 8 GHz and 4.63 W at 10.0 GHz. These results indicate that solar radiation should be considered since it may limit the APHC in circuits placed outside. The metal housing could be coated with white paint to increase the infrared emissivity up to ∼0.9, and consequently, to facilitate the cooling. The solar absorptivity of the white paint is assumed to be the same as that of the aluminum, i.e., 0.2. In this situation, the APHC is increased up to 15.51 and 4.94 W at 8 and 10.0 GHz, respectively. Note that for the atypical situation where $T_{\text{amb}} > T_{\text{ref}}$ the coating effect would be counter-productive, since the metal housing would absorb more infrared radiation from the environment due to the higher emissivity of the paint.

B. Example 2: First-Order Wideband Banstop Filter

By way of comparison, a filter topology similar to the previous one, but presenting a wider stopband bandwidth, has been analyzed. The structure is shown in Fig. 8, while its response is shown in Fig. 9. At the resonant frequency, i.e., at $f_0 = 10.0$ GHz, two standing waves are again formed,

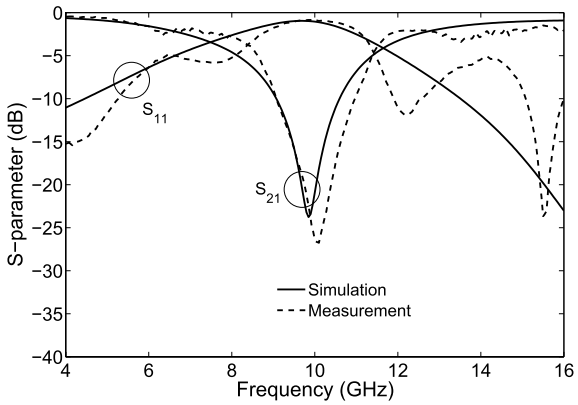

Fig. 9. Simulated and measured responses of the first-order wideband bandstop filter. Measured $BW_{10dB} = 18\%$.

one in the open-ended stub and another in the input feeding line. However, in this case, both the stub and the feeding lines present the same geometrical characteristics, leading to the same W_e and pair of attenuation constant values at 10 GHz ($\alpha_c = 0.13$ Np/m and $\alpha_d = 0.97$ Np/m). Thus, the hottest spots are going to be located on both parts of the circuit, as a difference from the previous filter, where the hottest spot is located on the stub. As deduced again from the attenuation coefficients, dielectric losses are more important than conductor losses at this frequency. As a consequence, the maximum ΔT values are to be found around the maximum points of electric field: 1) one in the stub open-circuited termination and 2) two more points along the input feeding line. Its predicted value is $\Delta T = 1.76$ °C/W. The ΔT is considerably lower than that of the previous filter, mainly due to its much wider W_e ($W_e = 3.80$ mm). The whole losses for this circuit are $Q_{\text{int}} = \Gamma P_{\text{in}} = 0.092 P_{\text{in}}$. This loss reduction with respect to the previous circuit can be explained by two different—but interrelated—ways: 1) the transmission lines involved in the current design present a lower global attenuation constant ($\alpha_c + \alpha_d$) and 2) losses are inversely proportional to the bandwidth. Fig. 10 shows the simulated and measured thermal profiles of the circuit under analysis at its resonance frequency and for the open metal housing configuration. As seen, there is again a good agreement between both results. In addition, the three aforementioned hottest spots can be clearly observed. Tables I and II briefly summarize the predicted, simulated, and measured results for both filters at their resonant frequencies. The measurements for the circuit in Example 2 were carried out with an ambient temperature of 24 °C, so that the predicted and simulated results were also computed at this temperature for this example. As deduced from these tables, increasing the operation bandwidth can substantially enhance the APHC.

The simulated APHCs given in Tables I and II are obtained by increasing P_{in} in the multiphysics simulator until T_{max} is reached in the simulation results. Regarding the provided measured APHCs, they are computed by linearly extrapolating the measured temperatures. If an uncertainty of δ °C is assumed in the thermal measurement results due to the uncertainties involved in the measurement setup (real convection

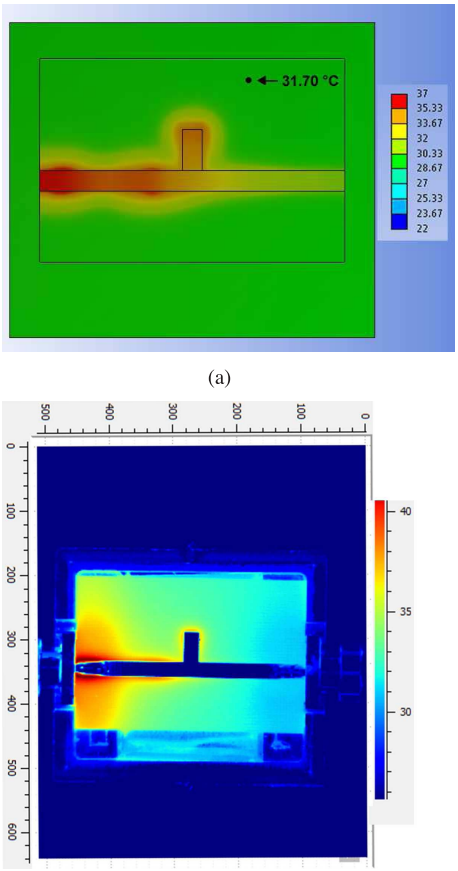

Fig. 10. (a) Simulated and (b) measured thermal profiles of the first-order wideband bandstop filter at 10.0 GHz for the open metal housing configuration.

TABLE I
SUMMARIZED RESULTS FOR EXAMPLE 1 AT 10 GHZ

Example 1	Open P; S; M	Enclosed P; S; M
T_{max} ($P_{in} = 2$ W)	46.8; 46.9; 50.1	44.9; 44.8; 48.5
T_{ref}($P_{in} = 2$ W)	31.2; 32.7; 33.4	29.3; 30.0; 31.2
APHC ($T_{max} = 80$ ^{o}C)	4.7; 4.8; 4.2*	5.1; 5.3; 4.8*

P stands for predicted; S for simulated and M for measured.
T_{ref} in measurements is calculated as the average temperature in the substrate area outside W_e.
*See comment provided at the end of Section III.

TABLE II
SUMMARIZED RESULTS FOR EXAMPLE 2 AT 10 GHZ

Example 2	Open P; S; M	Enclosed P; S; M
T_{max} ($P_{in} = 2$ W)	34.4; 36.2; 39.1	33.0; 35.5; 37.8
T_{ref}($P_{in} = 2$ W)	30.9; 31.7; 32.6	29.5; 30.6; 30.9
APHC ($T_{max} = 80$ ^{o}C)	10.7; 10.1; 7.6*	12.5; 11.8; 9.1*

P stands for predicted; S for simulated and M for measured.
T_{ref} in measurements is calculated as the average temperature in the substrate area outside W_e.
*See comment provided at the end of Section III.

coefficient, effective input power coming into the circuit, epoxy effect, etc.), the propagated uncertainty in the calculated APHC can be evaluated using, for example, the partial

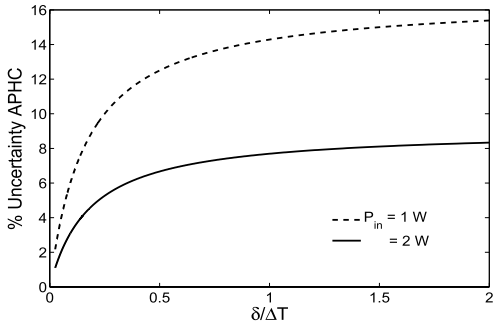

Fig. 11. Uncertainty (in %) on the measured APHC as a function of $\delta/\Delta T$, under varied P_{in}. In this example, $\delta = 1$ °C, $T_{\text{amb}} = 22$ °C, and $T_{\text{ref}} = 28$ (33) °C for $P_{\text{in}} = 1$ (2) W, respectively.

derivatives method. Fig. 11 shows the propagated uncertainty in the calculated APHC decreases as ΔT and the input power increase. Therefore, the higher ΔT and P_{in} are, the more accurate the measured APHC is.

IV. Conclusion

The APHC of microstrip passive circuits accounting for external conditions (such as convection and radiation heat transfer) and the metal housing effect has been studied and discussed in this paper. Closed-form equations and guidelines have been given to analyze all type of microstrip circuits in an easy and effective way. Two circuits have been analyzed in detail following the suggested method, and the results have been compared with those simulated and measured (with an infrared camera), showing a good agreement. In this paper, the external conditions can considerably reduce the APHC of microstrip circuits, and therefore they should be considered for a real-situation study. The influence of the layout and the electromagnetic behavior on the APHC as well as different ways to enhance the APHC have been also discussed.

References

[1] K. C. Gupta, R. Garg, I. J. Bahl, and P. Bhartia, *Microstrip Lines and Slotlines*, 2nd ed. Boston, MA, USA: Artech House, 1996.

[2] M. Yu, "Power-handling capability for RF filters," *IEEE Microw. Mag.*, vol. 8, no. 5, pp. 88–97, Oct. 2007.

[3] I. J. Bahl and K. C. Gupta, "Average power-handling capability of microstrip lines," *IEE J. Microw., Opt. Acoust.*, vol. 3, no. 1, pp. 1–4, Jan. 1979.

[4] W.-Y. Yin and X. T. Dong, "Wideband average power handling capability of coupled microstrips on polyimide and polyimide/GaAs substrates," *IEE Proc.-Microw., Antennas Propag.*, vol. 151, no. 5, pp. 385–392, Oct. 2004.

[5] W.-Y. Yin, X. Dong, and Y. B. Gan, "Frequency-dependent maximum average power-handling capabilities of single and edge-coupled microstrip lines on low-temperature co-fired ceramic (LTCC) substrates," *Int. J. RF Microw. Comput.-Aided Eng.*, vol. 16, no. 2, pp. 103–117, 2006.

[6] L.-S. Wu, X.-L. Zhou, W.-Y. Yin, M. Tang, and L. Zhou, "Characterization of average power handling capability of bandpass filters using planar half-wavelength microstrip resonators," *IEEE Microw. Wireless Compon. Lett.*, vol. 19, no. 11, pp. 686–688, Nov. 2009.

[7] L.-S. Wu, J. Mao, W.-Y. Yin, and M. Tang, "Average power handling capability of quarter-wavelength microstrip stepped-impedance resonator bandpass filter," in *IEEE MTT-S Int. Microw. Symp. Dig. (MTT)*, Jun. 2012, pp. 1–3.

[8] I. J. Bahl, "Average power handling capability of multilayer microstrip lines," *Int. J. RF Microw. Comput.-Aided Eng.*, vol. 11, no. 6, pp. 385–395, 2001.

[9] W.-Y. Yin and X. T. Dong, "Wide-band characterization of average power handling capabilities of some microstrip interconnects on polyimide and polyimide/GaAs substrates," *IEEE Trans. Adv. Packag.*, vol. 28, no. 2, pp. 328–336, May 2005.

[10] W.-Y. Yin, X. T. Dong, J. Mao, and L.-W. Li, "Average power handling capability of finite-ground thin-film microstrip lines over ultra-wide frequency ranges," *IEEE Microw. Wireless Compon. Lett.*, vol. 15, no. 10, pp. 715–717, Oct. 2005.

[11] W.-Y. Yin, K. Kang, and J.-F. Mao, "Electromagnetic-thermal characterization of on on-chip coupled (a)symmetrical interconnects," *IEEE Trans. Adv. Packag.*, vol. 30, no. 4, pp. 851–863, Nov. 2007.

[12] S. Lee, S. Song, V. Au, and K. P. Moran, "Constriction/spreading resistance model for electronics packaging," in *Proc. 4th ASME/JSME Thermal Eng. Joint Conf.*, vol. 4. 1995, pp. 199–206.

[13] Y. S. Muzychka, J. R. Culham, and M. M. Yovanovich, "Thermal spreading resistance of eccentric heat sources on rectangular flux channels," *J. Electron. Packag.*, vol. 125, no. 2, pp. 178–185, 2003.

[14] Y. S. Muzychka, "Influence coefficient method for calculating discrete heat source temperature on finite convectively cooled substrates," *IEEE Trans. Compon. Packag. Technol.*, vol. 29, no. 3, pp. 636–643, Sep. 2006.

[15] Y. A. Cengel and A. J. Ghajar, *Heat and Mass Transfer: Fundamentals and Applications*, 4th ed. New York, NY, USA: McGraw-Hill, 2011.

[16] V. Le Saux, Y. Marco, S. Calloch, P. Charrier, and D. Taveau, "Heat build-up of rubber under cyclic loadings: Validation of an efficient demarch to predict the temperature fields," *Rubber Chem. Technol.*, vol. 86, no. 1, pp. 38–56, 2013.

Miguel Á. Sánchez-Soriano (S'09–M'13) was born in Murcia, Spain, in 1984. He received the Telecommunications Engineer degree with a special award and the Ph.D. degree in electrical engineering from Miguel Hernandez University (UMH), Alicante, Spain, in 2007 and 2012, respectively.

He joined the Radiofrequency Systems Group at UMH as a Research Assistant in 2007. He was a Visiting Researcher with the Microwaves Group, Heriot-Watt University, Edinburgh, U.K., in 2010, and joined the Lab-STICC Group, Universit de Bretagne Occidentale, Brest, France, in 2013, as a Post-Doctoral Researcher, where he currently develops his research activities. His current research interests include analysis and design of microwave planar circuits, including reconfigurable filters and the multiphysics study of high-frequency devices.

Dr. Sánchez-Soriano serves as a reviewer for various journals and conferences, including the IEEE Transactions on Microwave, Theory and Techniques, the IEEE Microwave and Wireless Components Letters, and the *IET Microwaves, Antennas and Propagation*. He was a recipient of the Runner-Up HISPASAT Award to the Best Spanish Doctoral Thesis in New Applications for Satellite Communications from the Spanish Telecommunication Engineers Association.

Yves Queré (M'02) was born in Lannion, France, in 1980. He received the Electrical Engineer degree and the Ph.D. degree in electrical engineering from the University of Brest, Brest, France, in 2003 and 2006, respectively.

He has been an Assistant Professor with the Department of Electronic, University of Brest, since 2007. He was a Visiting Researcher with CNRS International NTU THALES Research Alliance, Nanyang Technological University, Singapore, in 2013. He is involved in research with the Microwaves Group, Lab-STICC Laboratory, Brest. His current research interests include microwave passive components (filters and antennas), and in particular, electromagnetic and multiphysics modeling.

Vincent Le Saux was born in Quimper (Finistre), France, in 1984. He received the Engineering degree in mechanical engineering from ENSTA Bretagne, Brest, France, in 2007, and the Ph.D. degree in mechanical engineering from the Université de Bretagne Occidentale, Brest, in 2010.

He joined the Mechanics of Materials and Assemblies Team, Brest Laboratory of Mechanics and Systems, Brest, in 2007, as a Research Assistant, the Heterogeneous Materials Behaviour Team, Brittany Laboratory of Engineering Materials, Lorient, France, in 2010, as a Post-Doctoral Researcher, and ENSTA Bretagne, in 2011, as an Assistant Professor, where he currently develops his research activities. He is also in charge of many equipments in the testing laboratory, including all infrared devices. His current research interests include analysis and prediction of the durability of polymers from experimental, modeling, and numerical points of view.

Cédric Quendo (M'03) was born in Plouay, France, in 1974. He received the Electrical Engineer degree and the Ph.D. degree in electrical engineering from the University of Brest, Brest, France, in 1999 and 2001, respectively.

He gave courses and conducted research at several institutes from 2001 to 2010. He was a Visiting Researcher with the Georgia Institute of Technology, Atlanta, GA, USA, in 2005. Since 2010, he has been a Professor with the Department of Electronics, University of Brest. He is also involved in research with the Microwaves Group, Lab-STICC Laboratory, Brest. His current research interests include modeling and design of microwave devices for microwave and millimeter-wave applications.

Stephane Cadiou, photograph and biography not available at the time of publication.